

Received August 27, 2020; reviewed; accepted December 22, 2020

The accurate algorithm of new surface area of single particle comminution, incorporating particle shape and roughness

Qing Guo ¹, Qiang Zhou ¹, Yongtai Pan ¹, Changyong Zhu ², Yinghua Wei ²

¹ China University of Mining and Technology Beijing, School of Chemical and Environmental Engineering, Beijing, 100083, China

² Shenhua Ningxia Coal Industry Group CO., LTD Taixi CPP, Ningxia Shi Zuishan 753000, China

Corresponding author: pan_yongtai@126.com (Yongtai Pan)

Abstract: Energy efficiency can be obtained by measuring accurate new surface energy in the crushing process. For the calculation of new surface energy, most researchers only pay attention to particle size distribution and ignore the influence of particle shape and roughness on the surface area. In this paper, the image processing technology was used to calculate the shape parameters and surface fractal dimension of the crushed granite sample. According to the different combinations of particle shape and roughness, the new surface area corresponding to the four basic models was calculated. For the surface area of a single particle, the calculation result of the rough model considering the surface fractal dimension is higher than that of the smooth model. Moreover, the ratio of the calculation results of the rough model and the smooth model increases significantly as the particle size increases. For 0.1 mm particles, the area ratio of the two models is 8, but for 25 mm particles, the area ratio reaches 130. In contrast, the particle shape is a secondary factor that affects the surface area calculation. The ellipsoidal model considering the particle shape has a surface area 30% larger than the spherical model. If the roughness and particle shape are considered when calculating the surface area, the energy efficiency of crushing is higher.

Keywords: crushing, surface area, particle shape, surface fractal dimension, calculation model, energy efficiency

1. Introduction

The energy consumption in the crushing process is enormous. The accurate calculation of energy efficiency can provide a basis for objective evaluation of crushing energy consumption. At the same time, it will lay a foundation for further research on the law of energy evolution in the crushing process. Accurate calculation of new surface energy (NSE) in the process of ore crushing is the key to obtain energy efficiency. The two factors that affect the NSE calculation are the new surface area (NSA) and surface free energy (SFE) (Sudarshan, 2016). The simplified method for calculating the NSA assumes that the crushed product is spherical particles, and the NSA is calculated according to the particle size distribution (PSD) before and after crushing (Hou et al., 2017; Jiang et al., 2013; Wang and Arson, 2018; Zhang et al., 2016). Although the spherical particle assumption makes the calculation of the surface area easier, it ignores the effect of particle shape and surface roughness on the actual surface area. Besides, when measuring the PSD of the coarse particles, a standard sieve is usually used. In general, the lower limit of the particle size for dry sieving using a standard sieve is 0.074 mm (Chen et al., 2012). Therefore, the PSD of particles smaller than this size cannot be obtained.

It is generally believed that the SFE is a constant related to the properties of the material, which can be estimated based on the fracture toughness, measured by contact angle experiments and scanning force microscopy (Calvimontes, 2017; Russell and Einav, 2013; Sauerer et al., 2016; Xie et al., 2015). However, in the field of geotechnical mechanics, to avoid the measurement of parameters that are not

easy to obtain, such as roughness, some scholars have calculated the energy dissipation indirectly by defining the fracture surface energy (Russell and Einav, 2013; Wang et al., 2020). The mineral processing field pays much attention to the energy efficiency of direct calculation. Therefore, this paper uses the contact angle method to obtain the SFE and calculate the NSE, although this method is sophisticated in operation.

To accurately calculate the NSE of the ore crushing process, particle shape and surface roughness should be considered. Moreover, it is necessary to calculate the particle size distribution of the full particle range. Li et al. (2010) measured the characteristics of rock burst debris, including the mass, length, width, and thickness of debris, and summarized the effective methods for measuring the mass and PSD of debris in different particle size ranges. For particles smaller than 0.074 mm, a laser particle size analyser was used to obtain PSD (Brown, 1985). Heywood (1947) established a method for measuring and evaluating the shape of crushed stone particles. The above studies provide methods for measuring particle shape, the relationship between particle shape and particle size.

In addition, the surface roughness of minerals is another important factor affecting the surface area. At present, the results of the gas adsorption method are relatively more accurate. However, limited by the size of the instrument, the optimal particle size range measured by the adsorption method is usually below 1 mm (Wang et al., 2020). Therefore, this method cannot measure the surface area of large particles. The application of fractal theory in characterizing roughness can make up for the limitation of the adsorption method for the measurement of larger particles.

Zhou and Xie (2003) used a laser profilometer to obtain the roughness data of the sandstone section to further determine the fractal dimension of the fracture surface. Xu and Sun (2005) used the image method to measure the surface fractal dimension and to characterize the roughness. Li et al. (2009) calculated the surface area of the rock material according to the product surface fractal dimension. Yanrong and Runqiu (2015) used various methods to measure the fractal dimension of rock fractures and studied its relationship with the joint roughness coefficient. Early research used the method of adding 1 to the perimeter fractal dimension (PFD) of the rough surface to approximate the surface fractal dimension (SFD) of the entire particle surface (Mandelbrot et al., 1984). In recent years, due to the development of scanning imaging equipment and the SFD calculation methods, direct measurement of rough surfaces has matured (Zhuang et al., 2005). Although direct analysis and measurement of rough surfaces can more fully characterize the surface fractal characteristics of particles, the testing process is tedious. In the face of a large number of samples, two-dimensional images are often used to study the surface fractal characteristics of particles (Li et al., 2019; Li and Huang, 2015).

In this study, the full size of the crushed particle was collected and analysed. The PSD of particles smaller than 0.3mm was measured by a laser particle size analyzer, and particles larger than 0.3mm were analyzed by a standard sieve. The contact angle method was used to measure the SFE of the granite. The data of the particle shape and the SFD were obtained by the image method. The variation law of the particle shape and the SFD of each size at different loading rates was studied. According to the combination of shape and roughness that affect the surface area of particles, surface area algorithms were divided into four categories. The differences in NSA calculated by different algorithms were compared, and the results were analyzed.

2. Fractal theory

The fractal dimension was first proposed by Hausdorff (1918) (also called Hausdorff dimension). Later, Mandelbrot (1975) generalized fractal dimension to form fractal geometry, which was used to deal with those extremely irregular shapes. In classical geometry, points are zero-dimensional, any curve is one-dimensional, and any curved surface is two-dimensional. This dimension takes only integer values, which is the dimension in the topological sense, called topological dimension D_T . The topological dimension reflects the number of independent coordinates or the number of independent directions required to determine the position of a point in space. The definition of a fractal is: if the Hausdorff dimension of a set is strictly greater than its topological dimension D_T , then the set is fractal, and fractal is a measure of the irregularity of graphics (Xie, 1996).

There are many fractal boundaries and fractal objects in nature. For example, the degree of irregularity in oceanic coastlines and in vertical sections of the Earth, the rough surface of crushed

minerals. For any smooth curve in Euclidean space, when measured with a yardstick ε , the following relationship can always be obtained:

$$L = N \cdot \varepsilon = \text{Constant} \quad (1)$$

where N is the number of measurements of yardstick ε required to measure L (length). The shape of many natural objects such as the length of the coastline and the length of the mineral profile lines are irregular and rough, and there is no such measurement relationship. In fact, the measured length can be approximated as:

$$L(\varepsilon) = L_0(\varepsilon/L_0)^{1-D} \quad (2)$$

where L_0 is a constant, and D is the fractal dimension of the curve. Generally, for a fractal curve $D > 1$, then:

$$\lim_{\varepsilon \rightarrow 0} L(\varepsilon) = L_0 \lim_{\varepsilon \rightarrow 0} (\varepsilon/L_0)^{1-D} = \infty \quad (3)$$

It shows that the length of the curve tends to infinite as the length of the yardstick approaches zero. If ε does not tend to zero, then:

$$\frac{\partial}{\partial \varepsilon} L(\varepsilon) = (1-D)(\varepsilon/L_0)^{-D} < 0 \quad (4)$$

This indicates that $L(\varepsilon)$ increases as the size ε decreases.

The fractal dimension D can describe the "roughness" of the curve (Lee et al., 1990). The larger D is, the more flexed and irregular the curve is; the smaller D is, the smoother the curve is. In other words, the fractal dimension D can quantitatively characterize the irregularity of the surface. The measurement equation of the fractal curve is extended to the multi-dimensional case, where n is the Euclidean dimension, and Eq. (2) can be generalized as:

$$G(\varepsilon) = G_0(\delta/\delta_{max})^{n-D} \quad (5)$$

Eq. (5) is suitable for measuring the fractal curve, fractal area, and fractal volume. Where n is Euclidean dimension, when $n = 1$, G and δ correspond to length; when $n = 2$, G and δ correspond to area and length; when $n = 3$, G and δ correspond to volume and length (Li and Deng, 1995). Therefore, the fractal surface area can be expressed as:

$$S = S_0(\delta_{min}/x)^{2-D_s} \quad (6)$$

where D_s is the SFD; x is the particle size; δ_{min} is the minimum yardstick length used to measure the fractal area; S_0 is the surface area of smooth particles. That is, $S_0 = k_s x^2$, and k_s is the surface shape factor, Eq. (6) shows that when the particle surface is smoother, $D_s \rightarrow 2.0$, and Eq. (6) is reduced to the classic surface area formula. The real mineral surface has a rich uneven structure, and the SFD can be used to characterize this fine structure.

3. Materials and methods

3.1. Material preparation

The granite used in the experiment was collected from Queshan of Henan in China. The granite was processed into a standard specimen with a 50 mm diameter and a height of 100 mm (Fig. 1). The two ends of the specimen were carefully ground with a grinder and sandpaper to make its parallelism, flatness, and perpendicularity meet the test requirements. The physical and mechanical parameters of the specimen are shown in Table 1. These parameters are determined in accordance with national standards, and at least three parallel tests were performed for each measurement.

3.2. Experimental device and particle size analysis method

The TAW-3000 hydraulic servo test system (Fig. 2a) was used to complete the uniaxial compression test of the granite specimen. The test system has a portal frame with a stiffness greater than 5 GN/m and can provide an axial force of 3000 kN. Five different loading rates (1 kN/s, 2 kN/s, 3 kN/s, 4 kN/s and 5 kN/s) were selected. Fig. 3 showed the maximum load corresponding to each loading rate. Three specimens were tested at the same conditions. A series of standard sieves (Fig. 2b) with specifications from 0.3 mm to 30 mm were selected to screen 15 groups of crushed products. The products were divided into -100+30 mm, -30+20 mm, -20+13 mm, -13+6 mm, -6+3 mm, -3+1 mm, -1+0.5 mm, -0.5+0.3

Table 1. Physical and mechanical parameters of granite specimen

Density/(g/cm ³)	Elasticity modulus /GPa	Poisson's ratio	Compressive strength /MPa
2.67	27.68	0.26	110.53



Fig. 1. Granite specimens

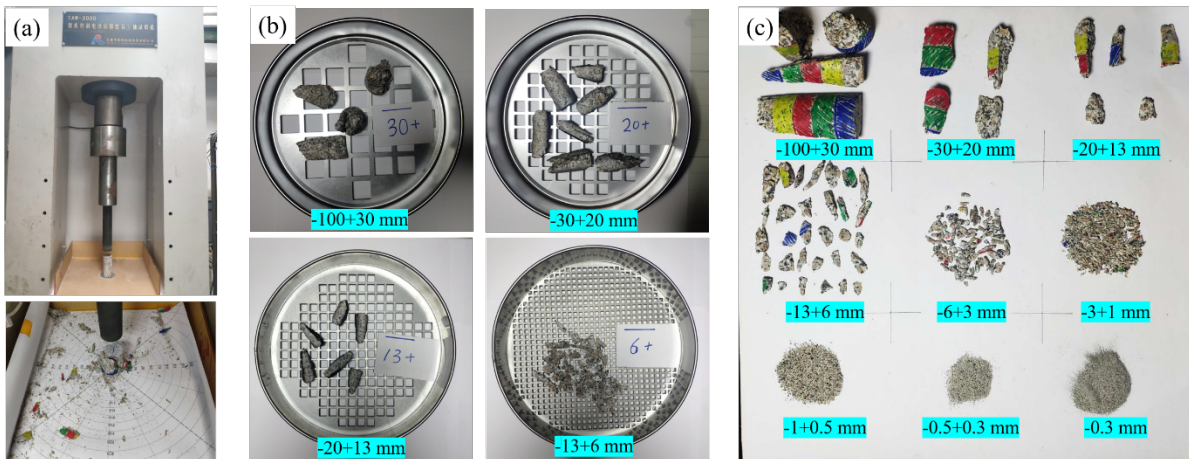


Fig. 2. Crushing and sieving of test specimens

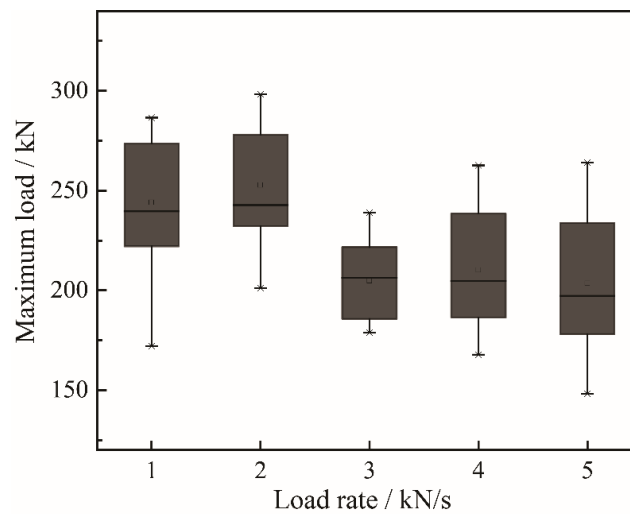


Fig. 3. Maximum load of different loading rate

mm, and -0.3 mm total 9 sizes (Fig. 2c). The EW-300A (accuracy is ± 0.0001 g) electronic balance was used to weigh the sieved products of each size, and the relative value of the weight loss of the products after sieving was less than 0.5%. The Malvern-MasterSizer 2000 laser particle size analyzer was used to measure the PSD of particles smaller than 0.3 mm.

3.3. Measurement of surface free energy

The granite was cut into cylindrical specimens with a diameter of 50 mm and a thickness of 10 mm using a cutting machine. The specimen surface was polished with 80 mesh, 120 mesh, 200 mesh, 500 mesh, and 1000 mesh sandpaper and then polished with a polishing machine. The contact angle of distilled water, formamide, diiodomethane, and the granite surface was measured by JY-82B video contact angle measuring instrument at room temperature (20 °C). Each experiment was measured 4 to 5 times, and then the average value was calculated (Table 2). According to the van Oss-Chaudhury-Good equation (Van Oss et al., 1988), the calculated SFE of granite is 58.996 mJ/m².

Table 2. Measurement results of granite contact angle at 20°C

Sample	Contact angle θ /(°)		
	Distilled water	Formamide	Diiodomethane
Granite	137.2 \pm 2.0°	77.4 \pm 0.5°	11.1 \pm 0.3°

3.4. Measurement of particle shape and surface fractal dimension

There were many indexes for evaluating the two-dimensional shape parameters of particles (Singh and Ramakrishnan, 1996). In this paper, three particle shape parameters elongation, flatness, and roundness were selected. The definitions of elongation, flatness, and roundness are shown in Table 3. The schematic diagram is shown in Fig. 4, where L , B , T stand for the length, breadth, and thickness of the particles. All three dimensions are normal to each other, measured at the particle in a stable position on a flat ground. A and P respectively represent the projected area and perimeter of the particles. Among the above particle shape parameters, elongation and flatness are values greater than or equal to 1, and roundness is less than or equal to 1.

Table 3. Shape parameters of crushed particles

Parameter name	Definition
Elongation (Heywood, 1947)	$El = L/B$
Flatness (Heywood, 1947)	$Fl = B/T$
Roundness (Wadell, 1932)	$S = 4A/\pi L^2$

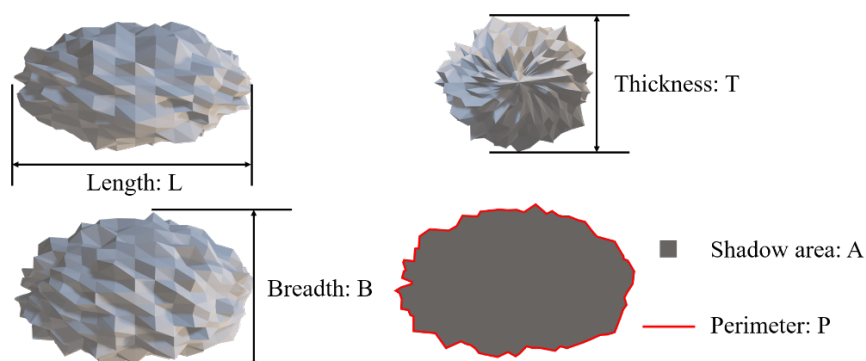


Fig. 4. Definition of shape parameters

Within the range that the camera resolution meets, the particles of four sizes (-100+30 mm, -30+20 mm, -20+13 mm, and -13+6 mm) were studied. Concerning the three-dimensional shape characteristic measurement system of particles (Li et al., 2019), a measurement system for the particle shape and SFD

of particles was designed (Fig. 5). The system consists of two support plates, a lighting system, and two cameras. A black calibration object of known size was placed on the support plate. A lighting system was installed on the bottom and sides of the device to eliminate shadows during image acquisition. Cameras were both fixed on the top and the side of the support plate to collect the particles' projected image from the vertical direction. The measurement process can be divided into the following steps. First, dye the particles into black with diluted ink and dry. Then, Place the particles on the support plate one by one according to the particle size, and take high-definition images with the camera system. Finally, import the image into Imagepro Plus to calculate the shape parameters and import it into MATLAB and use FracLab toolbox to get the PFD. The projected images of the particles are shown in Fig. 6.

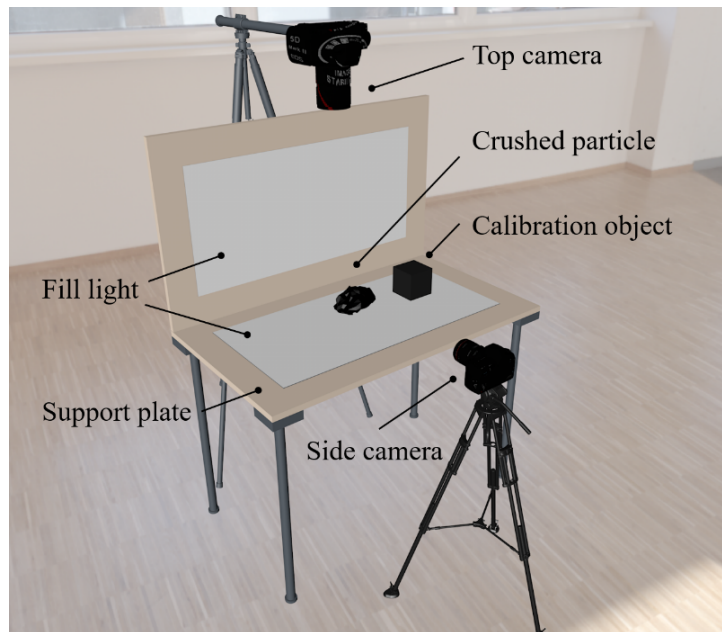


Fig. 5. Particle shape and fractal dimension measurement system

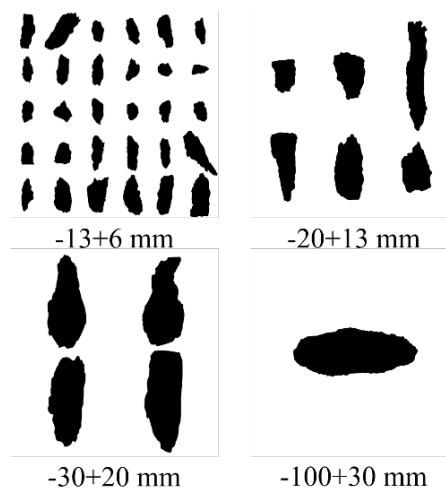


Fig. 6. Projection diagram of particles

4. Research results and discussion

4.1. The shape-size characteristics of crushed particles

The crushed particles were divided into five groups according to the loading rate. Each group contains 12 test specimens. The number and mass distribution data of the first group are shown in Table 4.

Table 4. Quantity and mass distribution of crushed products

Particle size /mm	Quantity / Block	Mass/g	Quantity percentage /%	Mass percentage /%
-100+30	31	3302.10	4.18	54.14
-30+20	57	1635.40	7.68	26.83
-20+13	65	564.92	8.76	9.26
-13+6	589	595.42	79.38	9.76
Total	742	6096.84	100	100

According to the calculation results in section 3.4, box plots of the elongation, flatness, and roundness of crushed particles with particle size under different loading rates are drawn, as shown in Figs. 7, 8, and 9.

Fig. 7 shows that the *El* of particles with a particle size range of -13+6 mm at different loading rates was not much different, around 2.5. For particles with a size range of -20+13 mm, lower loading rates the *El* was about 2.7, which was greater than the corresponding *El* of 2.0 at high-speed loading. For the -30+20 mm particles, the *El* was about 2~2.5. For the -100+30 mm particles, due to the size limitation of the specimen, and the median *El* was in the range of 1 ~ 2

Statistics show that the loading rate has little effect on the *El* from 6 to 13 mm, and the relationship between the *El* of the particles larger than 13 mm and the loading rate does not show regularity. For the quasi-static loading rate (1~5 kN/s) uniaxial compression experiment, the *El* of most of the particles falls within the range of 2~3. Liu et al. (2019) studied the length-width ratio of 4 grades of crushed stone particles of -5+2, -10+5, -20+10, -40+20 mm after the mechanical crushing of natural pebbles. The results show that the average *El* varies little with the size. The *El* of the crushed product has little correlation with the particle size, and the factors affecting the *El* may be the rock composition and the crushing method.

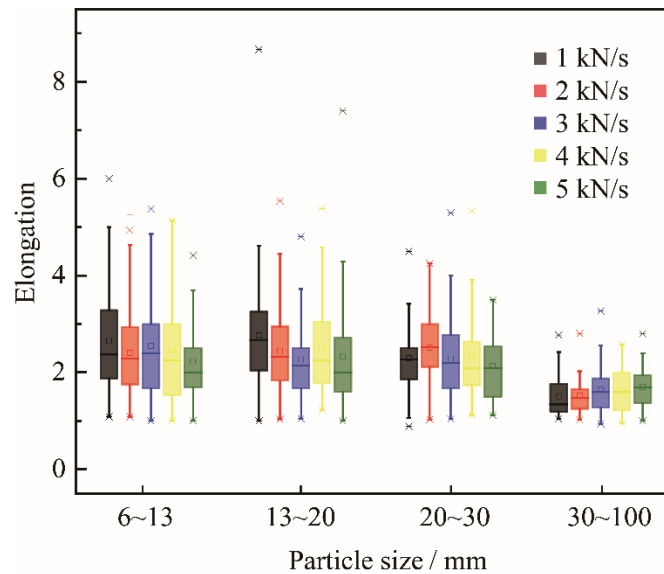


Fig. 7. Relationship between elongation and particle size at different loading rates

As shown in Fig. 8 that the *Fl* of the particles produced by different loading rates does not differ much, and the *Fl* and the particle size do not show a correlation. The *Fl* mostly falls within the range of 1.5~3.5. Compared with particles of other sizes, the *Fl* dispersion of particles larger than 30 mm is smaller, which may be caused by the size limitation of the test specimen. Similarly, in the study of morphology after crushing of coarse and fine aggregates, Rajan and Singh (2018) found that the difference in *Fl* of particles with different sizes produced by the same crushing method was not significant.

It can be seen from Fig. 9 that for the roundness of particles of 6 ~ 13 mm, the loading rate has little effect on it. The roundness range is mainly 0.77 ~ 0.86, and the median is 0.82. For particles of 13 ~ 20 mm the roundness at a loading rate of 3 kN/s is higher, with a median of 0.83, and the other loading

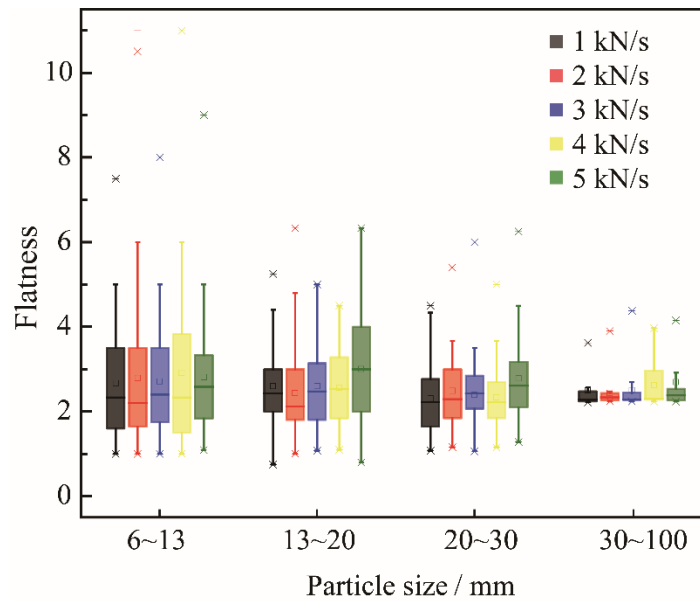


Fig. 8. Relationship between flatness and granularity at different loading rates

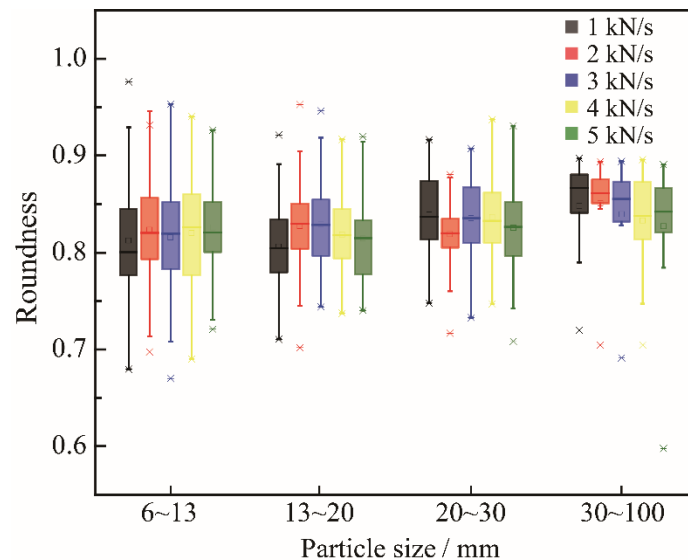


Fig. 9. Relationship between roundness and granularity at different loading rates

rates correspond to a median of 0.8 to 0.82. For particles of 20 ~ 30 mm, the median roundness falls within the range of 0.81 ~ 0.85. The roundness of particles bigger than 30 mm mainly distributed in the interval of 0.83~0.87. Similarly, in the study of the roundness of 9.5~62.5 mm (full size) grain granite, Pen et al. (2013) found that the discrepancy of roundness of different sizes are slight, and the roundness coefficient is between 0.8 and 0.98.

4.2. The surface fractal dimension and size characteristics of crushed particles

As shown in Fig. 10, the PFD of the crushed particles has a positive correlation with the particle size, while it is not much affected by the loading rate. It is observed that the PFD of particles in $-13+6$ mm is 1.79~1.81; the PFD of particles in $-20+13$ mm is 1.80~1.82; the PFD of particles in $-30+20$ mm is 1.81~1.83; the PFD of particles larger than 30 mm is 1.82~1.85. At present, the research on the relationship between the fractal dimension of crushed particles and particle size is not comprehensive enough. Researchers usually use a method to measure particles' fractal dimension in a specified particle size range of a specific mineral. Therefore, the conclusions drawn have certain limitations. Li et al. (1997) used the divider method to measure the fractal dimension of the periphery of $-0.9+0.074$ mm particles. They

found that the average value of PFD decreased with the increase of particles, that is, fine-grained minerals have complex surfaces. Lin et al. (2020) used the box dimension method to study the fractal dimension of the crystal profile of gypsum broken in different ways. The results showed that the fractal dimension was between 1.79 and 1.96. Ge et al. (2014) found that the fractal dimension of the profile was 1.09~1.14 when using a laser scanning method to study the roughness of natural rock joints. Given the above research results, it is still impossible to determine the relationship between the surface fractal dimension and the particle size of the broken rock. In theory, the surface fractal dimension can range from 2.0 to 3.0 (Giorgio and Daniele, 2007).

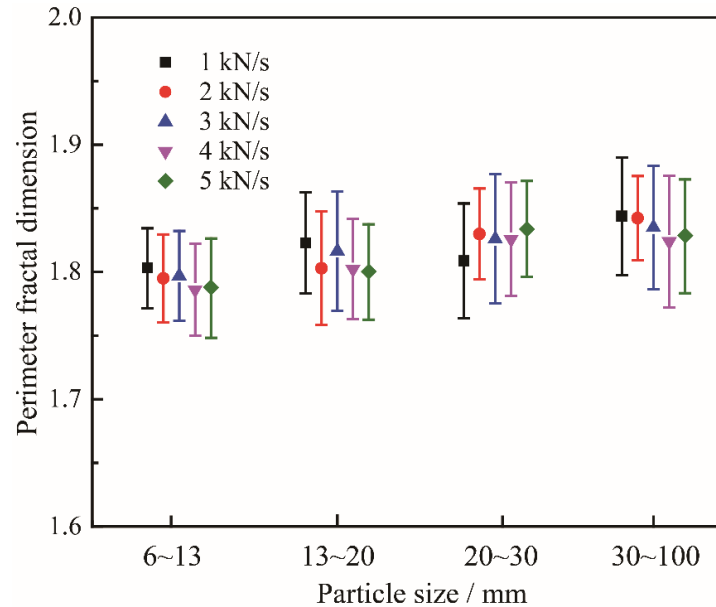


Fig. 10. The relationship between PFD and particle size at different loading rates

4.3. Comparison of different new surface area algorithms

The surface area calculation algorithms can be divided into four types according to the differences in the factors that affect the particle surface area. They are the smooth sphere (SS) model, smooth ellipsoid (SE) model, rough sphere (RS) model, and rough ellipsoid (RE) model, as shown in Fig. 11. In the SS Model, the surface area of a single particle is the surface area of a sphere of the same mass. In the SE Model, it is necessary to use the elongation and flatness indicators obtained in 4.1 to calculate the surface area of the ellipsoid with the same mass. The RS Model considers the influence of roughness on the surface area based on a smooth sphere.

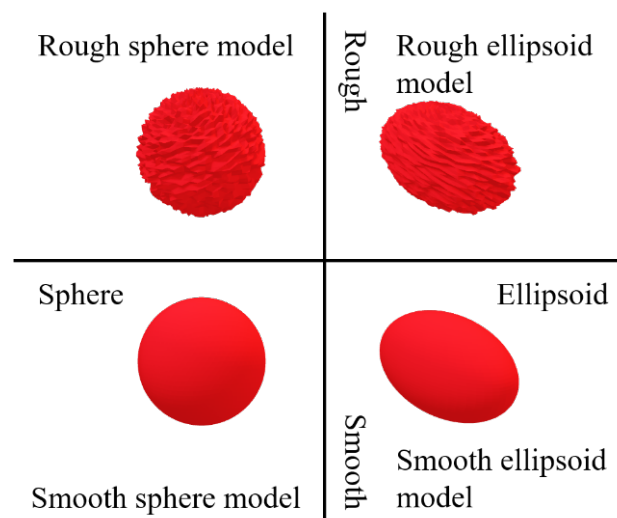


Fig. 11. Different calculation models of particle surface area

Given the current controversy on the relationship between fractal dimension and particle size, and the surface fractal dimension ranges from 2.0 to 3.0 in theory. In this calculation, a total of 5 fractal dimensions are selected, that is 2.1, 2.3, 2.5, 2.7, and 2.9. Then, calculate the particle surface area by Eq. (5). The minimum particle size interval measured in this experiment was $-4+2 \mu\text{m}$, so the equivalent diameter of the particle in this interval was selected as the minimum yardstick length δ_{min} for measuring the fractal surface area (Ji et al., 2009). The RE Model is based on the SE Model considering the effect of roughness, the selection and calculation method of fractal dimension are consistent with the RS Model. According to the algorithms mentioned above and the PSD data of the No. 5 test specimen, the single particles of each particle size and the total area were calculated, and the area-size distribution diagrams are drawn (Figs. 12 and 14). The PSD data is shown in Tables 6 and 7.

Table 6. Test specimen No.5 PSD data of crushed products (using sieve method)

Size range /mm	Total mass /g	Number of particles	Single particle mass/g
-100+30	305.573	3	101.877
-30+20	71.101	4	17.775
-20+13	41.062	6	6.844
-13+6	40.410	38	1.063
-6+3	18.483	233	0.079
-3+1	17.839	997	0.018
-1+0.5	12.672	8361	0.0015
-0.5+0.3	5.434	54246	0.0001

Table 7. Test specimen No.5 PSD data of crushed products (using laser diffraction particle size analyzer)

Size range / μm	Total mass /mg	Number of particles (10^3)	Single particle mass/ng
-256+128	2516.33	305.554	8230
-128+64	1734.17	1572.545	1100
-64+32	766.64	5095.74	150
-32+16	237.75	12412.7	19
-16+8	78.12	33702.3	2.3
-8+4	44.96	174258	2.58×10^{-1}
-4+2	36.82	1173215	3.14×10^{-2}

The left axis of Fig. 12 represents the surface area of a single particle, and the right axis is the surface ratio between different calculation models. For convenience, the simplest SS Model was used as a benchmark for comparison. As shown in Fig. 12 that the surface area-particle size curve of the SS Model and the SE Model are relatively close. Similarly, the surface area-particle size curve of the RS Model and the RE Model are relatively close. However, for the same particle shape, the rough model was different from the smooth model. To some extent, the fractal dimension had a more significant influence on the surface area calculation results. Besides, the area ratio of the right axis indicates that the area ratio of large particles is significantly larger than that of small particles when considering the SFD. For particles with a size of $100 \mu\text{m}$, the surface area calculated by the RE Model is ten times that of the SS Model. For particles with a size of 20 mm , the ratio of the surface area calculated by the RE Model to the SS Model is close to 150. However, the area ratio of each particle size of the SE Model to the SS Model is a constant, which is consistent with the elongation and flatness selected by the calculation model. The elongation and flatness of this ellipsoid model are both 2.5; therefore, the corresponding surface area ratio coefficient is 1.3.

To avoid the curve in Fig. 12 from being too confusing, the SFD selected by the rough model was 2.5. Fig. 13a shows the area-size distribution of single particles under different SFD of the RS Model. It can be found that the larger the SFD, the larger the surface area. To facilitate the comparison of the influence of different SFD on the surface area, the area ratio of the RS Model to the SS Model under different SFD is calculated (Fig. 13b). Fig. 13b shows that the area of a $-6+3 \text{ mm}$ particle with a fractal dimension of 2.9 is that of a particle with a fractal dimension of 2.0 (smooth particle) 1000 times. Obviously, with the

increase of the fractal dimension, the fractal dimension gradually becomes the main factor affecting the surface area calculation, and its influence is far more significant than the particle shape. Since it is currently impossible to obtain the value of the full-grain fractal dimension, the following calculation uses the fractal dimension 2.5 as the calculation standard.

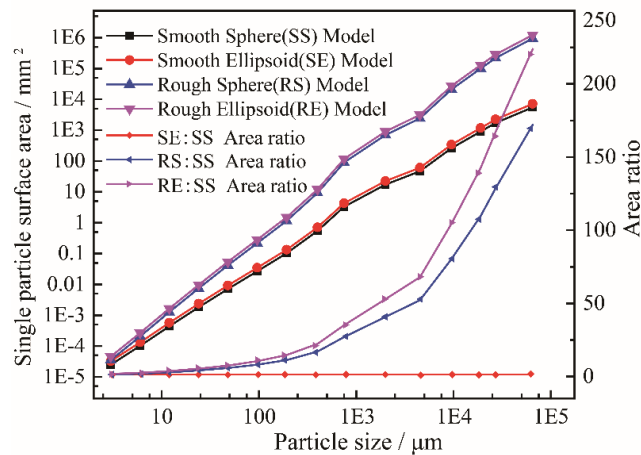


Fig. 12. Single particle surface area-size distribution

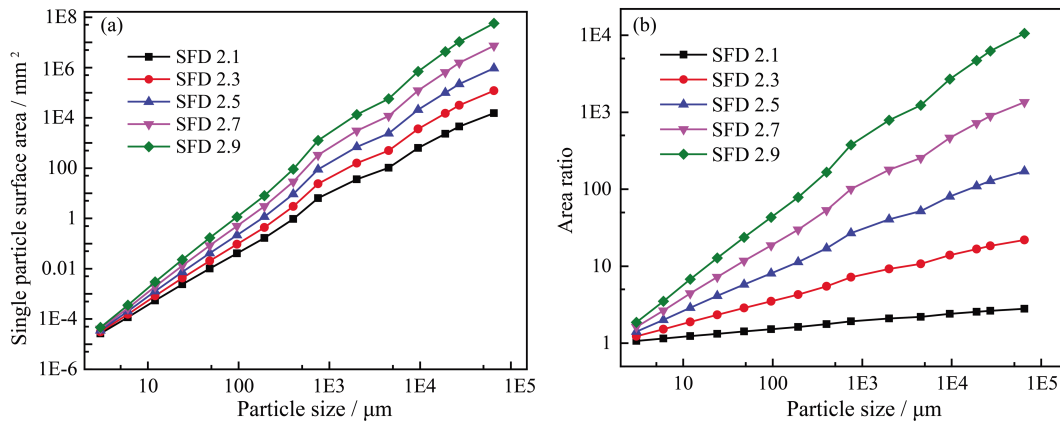


Fig. 13. Single particle surface area -size distribution with different SFD

According to the single particle surface area and the number of particles of each size, the total surface area-particle size distribution can be obtained (Fig. 14). The left axis of the Fig. 14a is the total surface area of all particles in the corresponding size, and the right axis is the number of particles. The total surface area of different calculation models shows different trends with the change of particle size. Since the total surface area calculated by the smooth model is small, the changing trend cannot be clearly observed in Fig. 14a, so it is listed separately in Fig. 14b. Because the particle shape has little influence on the area calculation, and the particle shape parameter does not change with the size in the algorithm. Only the influence of roughness on the results is discussed here. As shown in Fig. 14a, the difference between the smooth model and the rough model is not obvious for particles smaller than 10 μm. In the rough model, from 10 to 1000 μm, the total surface area of each particle size increases with the increase of particle size. In the range of 20-1 mm, the total surface area fluctuates slightly around 1 m². The total surface area of particles larger than 30 mm rises suddenly, and the area of the RE Model exceeds 3.5 m². There is a peak at 100 μm, and the corresponding area is 0.055 m², much less than 3.5 m² of the rough model (Fig. 14b).

To conveniently compare the contribution of the surface area of each particle size to the overall surface area, the ratio of the surface area of each particle size is obtained (Fig. 15). In the smooth model, 100 μm size particles contribute the most to the total surface area, with a contribution rate of 14%. While in the rough model, particles larger than 30 mm contribute the most to the total surface area, exceeding 30% of the total surface area. Besides, the SS Model and SE Model area ratio curves, the RS Model and

RE Model area ratio curves coincide. This phenomenon is caused by the fact that the particle shape parameter does not change with the size in the algorithm, that is, the particle shape parameter does not change the proportion of each particle size contribution to the surface area.

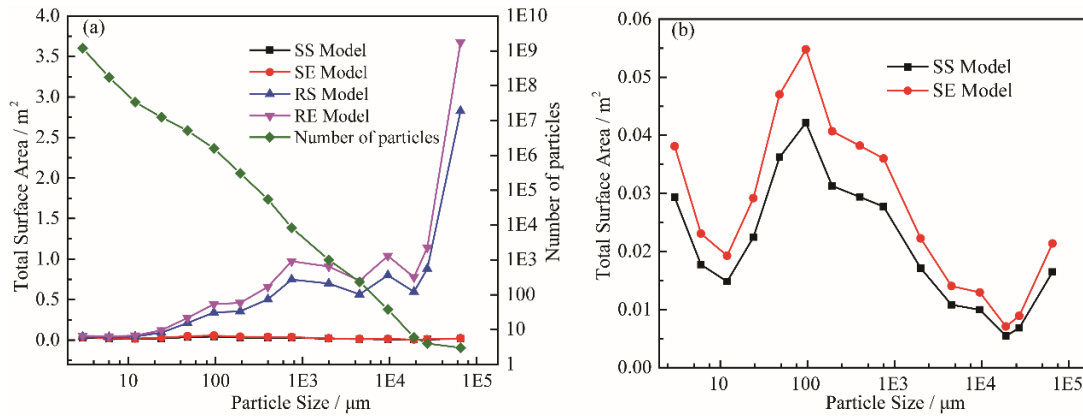


Fig. 14. Total surface area-size distribution

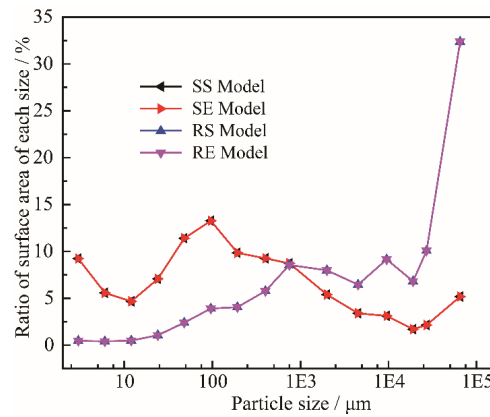


Fig. 15. Contribution ratio of surface area contribution of each model in different models

The total surface area of the particles calculated by the four models: SS Model, SE Model, RS Model (SFD 2.5), and RE Model (SFD 2.5) are shown in Table 8. The surface energy is 58.996 mJ/m². It is easy to calculate NSE. As shown in the table, when the particle shape is the same, the NSE of the rough model is 27 times that of the smooth model. In the same roughness, the NSE of the ellipsoid model is 1.3 times that of the sphere model.

Table 8. Surface area and NSE of different model

Model	Surface area / m²	NSE / mJ
SS Model	0.32	19.05
SE Model	0.41	24.76
RS Model (SFD 2.5)	8.73	523.86
RE Model (SFD 2.5)	11.35	681.01

5. Conclusions

This paper used the image method to study the relationship between the shape and roughness of the crushed granite product and the product size and loading rate. The differences between the four different new surface area algorithms were compared.

The loading rate of the granite uniaxial compression process and the product size had no significant influence on the particle shape. The SFD was not greatly affected by the loading rate. In the range of -100+6 mm, the fractal dimension of the particle surface increased with the increase of particle size.

The rough model was more significantly different from the smooth model when calculating the surface area of large particles. For 10 μm particles, the calculation result of the rough model was four times that of the smooth model, while for the 20 mm particles, the difference was 140 times. Therefore, large particles contributed more to the total surface area in the rough model.

If the particle shape and roughness are considered when calculating the particle surface area, higher energy efficiency will be obtained. In addition, roughness has a more significant effect on the surface area than particle shape. When the particle shape was the same, the NSE of the rough model was 27 times that of the smooth model; when the roughness was the same, the NSE of the ellipsoid model was 1.3 times that of the sphere model.

To make the calculation results more accurate, it is necessary to systematically measure the SFD of each size of the crushed product.

Acknowledgments

The financial support from National Natural Science Foundation of China (Grant No. 52074308) and Shenhua Ningxia Coal Industry Group Co., Ltd. Taixi Coal Preparation Plant, Shi zuishan Ningxia 753000, China.

List of symbols

NSE	New surface energy
NSA	New surface area
SFE	Surface free energy
PSD	Particle size distribution
PFD	Perimeter fractal dimension
SFD	Surface fractal dimension
SS	Smooth sphere
SE	Smooth ellipsoid
RS	Rough sphere
RE	Rough ellipsoid

References

- BROWN, D. J., 1985. *Direct measurement of concentration and size for particles of different shapes using laser light diffraction*. Chem.eng.res.des 63, 125-132.
- CALVIMONTES, A., 2017. *The measurement of the surface energy of solids using a laboratory drop tower*. Npj Microgravity 3
- CHEN, X., WANG, S. Z., LI, L., 2012. *Characteristics of fragments of jointed rock mass model under uniaxial compression*. Chinese Journal of Rock Mechanics and Engineering 31, 898-907.
- GE, Y. F., KULATILAKE, P. H. S. W., TANG, H. M., XIONG, C. R., 2014. *Investigation of natural rock joint roughness*. Computers and Geotechnics 55, 290-305.
- GIORGIO, F., DANIELE, R., 2007. *SCATTERING, NATURAL SURFACES, AND FRACTALS*. London, Academic Press.
- HAUSDORFF, F., 1918. *Dimension und äußeres Maß*. Mathematische Annalen 79, 157-179.
- HEYWOOD, H., 1947. *Symposium on particle size analysis*. Trans. Inst. Chem. Eng, 14.
- HOU, T. X., XU, Q., XIE, H. Q., XU, N. W., ZHOU, J. W., 2017. *An estimation model for the fragmentation properties of brittle rock block due to the impacts against an obstruction*. Journal of Mountain Science 14, 1161-1173.
- JI, T., HU, C. B., LI, X. J., 2009. *Simplified calculation method of specific surface area of coarse aggregate based on fractal theory*. Concrete, 27-28.
- JIANG, H. X., DU, C. L., LIU, S. Y., 2013. *The effects of impact velocity on energy and size distribution of rock crushing*. JOURNAL OF CHINA COAL SOCIETY 38, 604-609.
- LEE, Y. H., CARR, J. R., BARR, D. J., HAAS, C. J., 1990. *The fractal dimension as a measure of the roughness of rock discontinuity profiles*. International Journal of Rock Mechanics Mining Sciences & Geomechanics Abstracts 27, 453-464.

- LI, D. J., JIA, X. N., MIAO, J. L., HE, M. C., LI, D. D., 2010. *Analysis of fractal characteristics of fragment from rockburst test of granite*. Chinese Journal of Rock Mechanics and Engineering 29, 3280-3289.
- LI, G. B., CHEN, Q. S., XU, X. H., 1997. *Fractal in Rock Fracture*. Beijing, Seismological Press.
- LI, G. Q., DENG, X. J., 1995. *Fractal effect of graded aggregate*. Concrete 1, 3~7.
- LI, L. Y., JU, Y., ZHAO, Z. W., WANG, L., LU, J., MA, X., 2009. *Energy analysis of rock structure under static and dynamic loading conditions*. JOURNAL OF CHINA COAL SOCIETY 34, 737-740.
- LI, R. Z., LU, W. B., YIN, Y. J., YU, Y. J., CHEN, M., XIA, W. J., YAN, P., 2019. *Study on the shape and specific surface area characteristics of blasting gravel particles of limestone in Hangudi quarry of Baihetan*. Chinese Journal of Rock Mechanics and Engineering 38, 1344-1354.
- LI, Y. R., HUANG, R. Q., 2015. *Relationship between joint roughness coefficient and fractal dimension of rock fracture surfaces*. International Journal of Rock Mechanics Mining Sciences 75, 15-22.
- LIN, M. Q., ZHANG, L., LIU, X. Q., XIA, Y. Y., HE, J. Q., KE, X. S., 2020. *The Meso-Analysis of the Rock-Burst Debris of Rock Similar Material Based on SEM*. Advances in Civil Engineering 2020, 1~13.
- LIU, G., ZHAO, M. Z., LU, R., LUO, Q., LU, C., 2019. *Morphology characteristics of gravel particle and its relationship with stacking void ratio*. Rock and Soil Mechanics 40, 4644-4651.
- MANDELBROT, B. B., 1975. *Stochastic models for the Earth's relief, the shape and the fractal dimension of the coastlines, and the number-area rule for islands*. Proceedings of the National Academy of Sciences of the United States of America 72, 3825-3828.
- MANDELBROT, B. B., PASSOJA, D. E., PAULLAY, A. J., 1984. *Fractal character of fracture surfaces of metals*. Nature 308, 721-722.
- PEN, L. M. L., POWRIE, W., ZERVOS, A., AHMED, S., AINGARAN, S., 2013. *Dependence of shape on particle size for a crushed rock railway ballast*. Granular Matter 15, 849-861.
- RAJAN, B., SINGH, D., 2018. *Investigation on effects of different crushing stages on morphology of coarse and fine aggregates*. International Journal of Pavement Engineering 21, 177-195.
- RUSSELL, A. R., EINAV, I., 2013. *Energy dissipation from particulate systems undergoing a single particle crushing event*. Granular Matter 15, 299-314.
- SAUERER, B., STUKAN, M., ABDALLAH, W., DERKANI, M. H., FEDOROV, M., BUTTING, J., ZHANG, Z. J., 2016. *Quantifying mineral surface energy by scanning force microscopy*. Journal of Colloid Interface Science 472, 237-246.
- SINGH, P., RAMAKRISHNAN, P., 1996. *Powder Characterization by Particle Shape Assessment*. KONA 14, 16-30.
- SUDARSHAN, M., 2016. *Size-energy relationship in comminution, incorporating scaling laws and heat*. International Journal of Mineral Processing 153, 29-43.
- VAN OSS, C. J., GOOD, R. J., CHAUDHURY, M. K., 1988. *Additive and nonadditive surface tension components and the interpretation of contact angles*. Langmuir 4, 884-891.
- WADELL, H., 1932. *Volume, Shape, and Roundness of Rock Particles*. The Journal of Geology, 443-451.
- WANG, C. H., CHENG, Y. P., YI, M. H., HU, B., JIANG, Z. N., 2020. *Surface energy of coal particles under quasi-static compression and dynamic impact based on fractal theory*. Fuel 264, 1-12.
- WANG, P., ARSON, C., 2018. *Energy distribution during the quasi-static confined comminution of granular materials*. Acta Geotechnica 13, 1-9.
- XIE, H. P., 1996. *Fractal: An Introduction to Rock Mechanics*. Beijing, Science Press.
- XIE, Y. J., WANG, X. H., HU, X. Z., ZHU, X. Z., 2015. *Fracture-based model of periodic-arrayed indentation for rock cutting*. International Journal of Rock Mechanics Mining Sciences 76, 217-221.
- XU, Y. F., SUN, D. A., 2005. *Correlation of surface fractal dimension with frictional angle at critical state of sands*. Geotechnique 55, 691-695.
- YANRONG, L., RUNQIU, H., 2015. *Relationship between joint roughness coefficient and fractal dimension of rock fracture surfaces*. International Journal of Rock Mechanics Mining Sciences 75, 15-22.
- ZHANG, C. S., NGUYEN, G. D., KODIKARA, J., 2016. *An application of breakage mechanics for predicting energy-size reduction relationships in comminution*. Powder technology 287, 121-130.
- ZHOU, H. W., XIE, H. P., 2003. *Direct Estimation of the Fractal Dimensions of a Fracture Surface of Rock*. Surface Review Letters 10, 751-762.
- ZHUANG, Y. H., ZHOU, H. W., XIE, H. P., 2005. *Improved cubic covering method for fractal dimensions of a fracture surface of rock*. Chinese Journal of Rock Mechanics and Engineering 24, 3192-3196.